HHS Public Access

Author manuscript

Eur J Radiol. Author manuscript; available in PMC 2023 October 23.

Published in final edited form as:

Eur J Radiol. 2022 November ; 156: 110515. doi:10.1016/j.ejrad.2022.110515.

Low-field 0.55 T MRI for assessment of pulmonary groundglass and fibrosis-like opacities: Inter-reader and inter-modality concordance

Lea Azour[a,*], **Rany Condos**[b], **Mahesh B. Keerthivasan**[c], **Mary Bruno**[a], **Terlika Pandit Sood**[a], **Nicholas Landini**[d], **Quinn Silverglate**[e], **James Babb**[a], **Hersh Chandarana**[a], **William H. Moore**[a]

[a]Department of Radiology, NYU Grossman School of Medicine, NYU Langone Health, New York, NY, USA

[b]Division of Pulmonary, Sleep and Critical Care Medicine, Department of Medicine, NYU Grossman School of Medicine, NYU Langone Health, New York, NY, USA

[c]Siemens Medical Solutions USA Inc, New York, NY, USA

[d]Department of Radiological Sciences, Oncology and Pathology, Sapienza University/Policlinico Umberto, Rome, Italy

[e]NYU Grossman School of Medicine, NYU Langone Health, New York, NY, USA

Abstract

Purpose: To evaluate detection and characterization of groundglass and fibrosis-like opacities imaged by non-contrast 0.55 Tesla MRI, and versus clinically-acquired chest CT images, in a cohort of post-Covid patients.

Materials and methods: 64 individuals (26 women, mean age 53 ± 14 years, range 19–85) with history of Covid-19 pneumonia were recruited through a survivorship registry, with 106 non-contrast low-field 0.55 T cardiopulmonary MRI exams acquired from 9/8/2020–9/28/2021. MRI exams were obtained at an average interval of 9.5 ± 4.5 months from initial symptom report (range 1–18 months). Of these, 20 participants with 22 MRI exams had corresponding clinically-acquired CT chest imaging obtained within 30 days of MRI (average interval 18 ± 9 days, range 0–30). MR and CT images were reviewed and scored by two thoracic radiologists, for presence and extent of lung opacity by quadrant, opacity distribution, and presence versus absence of fibrosis-like subpleural reticulation and subpleural lines. Scoring was performed for each of

[*]Corresponding author. Lea.Azour@nyulangone.org (L. Azour).

Declaration of Competing Interest

The authors declare that they have no known competing financial interests or personal relationships that could have appeared to influence the work reported in this paper.

Peer review under responsibility of If file “editor conflict of interest statement” is present in S0, please extract the information and add it as a footnote (star) to the relevant author. The sentence should read (and be amended accordingly): Given his/her role as EditorinChief/Associate Editor/Section Editor <NAME of Editor> had no involvement in the peerreview of this article and has no access to information regarding its peerreview.

Appendix A. Supplementary material

Supplementary data to this article can be found online at https://doi.org/10.1016/j.ejrad.2022.110515.

four lung quadrants: right upper and middle lobe, right lower lobe, left upper lobe and lingula, and left lower lobe. Agreement between readers and modalities was assessed with simple and linear weighted Cohen's kappa (k) coefficients.

Results: Inter-reader concordance on CT for opacity presence, opacity extent, opacity distribution, and presence of subpleural lines and reticulation was 99%, 78%, 97%, 99%, and 94% (k 0.96, 0.86, 0.94, 0.97, 0.89), respectively. Inter-reader concordance on MR, among all 106 exams, for opacity presence, opacity extent, opacity distribution, and presence of subpleural lines and reticulation was 85%, 48%, 70%, 86%, and 76% (k 0.57, 0.32, 0.46, 0.47, 0.37), respectively. Inter-modality agreement between CT and MRI for opacity presence, opacity extent, opacity distribution, and presence subpleural lines and reticulation was 86%, 52%, 79%, 93%, and 76% (k 0.43, 0.63, 0.65, 0.80, 0.52).

Conclusion: Low-field 0.55 T non-contrast MRI demonstrates fair to moderate inter-reader concordance, and moderate to substantial inter-modality agreement with CT, for detection and characterization of groundglass and fibrosis-like opacities.

Keywords

Low-field MRI; .55T; Groundglass opacities; Fibrosis-like; pulmonary

1. Introduction

Lung parenchymal evaluation on magnetic resonance imaging (MRI) is challenged by several factors, chiefly signal characteristics inherent to lung tissue, respiratory motion, long exam acquisition times, and accessibility. While current Fleischner Society recommendations support the clinical use of pulmonary MRI for indications including cystic fibrosis, lung cancer staging, and lung nodule characterization, further investigation is needed prior to clinical integration of MRI for the evaluation of other pulmonary parenchymal abnormalities [1].

Lung parenchyma has low proton density, resulting in low T1 and T2 signal intensity. Air-tissue interfaces also create signal decay and susceptibility artifact, further limiting detection and characterization of lung pathology. Several strategies to augment lung signal include the development of ultrashort echo time (UTE) T1-weighted images [2–7], fast or turbo spin-echo (TSE) T2-weighted imaging [8–10], and the use of low-field strength [9].

Low-field strength increases T2 time and shortens T1 relaxation, thereby increasing signal intensity. T2* is also prolonged for lung parenchyma at lower field strengths, reducing magnetic susceptibility artifacts due to local field inhomogeneity, such as at air-tissue interfaces in lung [11]. These features may augment visualization of fine detail in the lung, as well as any superimposed pathology, including groundglass opacities. Illustration of groundglass opacities on low-field 0.55 T MRI has been demonstrated in case reports of patients with Covid-19 [12,13]. Patients who recover from Covid-19 may have persisting lung parenchymal opacities. These opacities have been shown to decrease over time, yet have been reported to persist in 25 % of individuals one year after diagnosis [14]. Reported opacities on computed tomography (CT) are primarily groundglass in attenuation, and most

suggestive of resolving or residual lung injury given similarity in distribution to acute/earlier phase of illness [15].

The purpose of this pilot study was to evaluate the detection and characterization of groundglass opacities imaged by non-contrast 0.55 T MRI, and in comparison to clinically-acquired chest CT images, in a cohort of post-Covid patients.

2. Methods

2.1. Patient selection

Patients were recruited through our institution's Covid-19 Survivorship Registry, a HIPAA-compliant registry approved by our institutional review board, and for which all subjects provided written informed consent. The registry was open to all patient with history of Covid-19 infection, with accrual beginning with admitted patients during the first Covid-19 surge in New York City in March 2020.

A retrospective review of all low-field 0.55 T cardiopulmonary MRI exams acquired from 9/8/2020 through 9/28/2021 was performed, yielding 106 MRI examinations in 64 patients. All low-field MRI examinations were performed on an outpatient basis. Chest CT imaging (obtained for clinical purposes) was performed within 30 days of MRI in 20 patients, two of whom had two exams. These 22 paired MR and CT exams were used for inter-modality analyses. All available MRI exams were used for inter-reader analyses.

2.2. MRI acquisition parameters

A commercial MRI system (1.5 T MAGNETOM Aera; Siemens Healthcare, Erlangen, Germany) was modified to operate as a research prototype system at 0.55 T field strength, using 6-channel anterior body array and 18-channel spine array coils. Pulmonary imaging sequences included axial breath-hold (BH) bSSFP/TRUFI, 2D coronal free-breathing bSSFP/TRUFI, and axial navigator-triggered T2 turbo-spin-echo (TSE) sequence with radial, motion insensitive, trajectory sampling (BLADE, Supplementary Table 1).

The non-contrast sequences were optimized follows:

a. A balanced SSFP (bSSFP/TRUFI) sequence based three-plane localizer was used for fast BH T2-weighted imaging to overcome the poor signal to noise ratio (SNR) observed in single-shot fast spin-echo sequence.

b. This was followed by a coronal free breathing non-fat suppressed 2D bSSFP/TRUFI acquisition for pulmonary vasculature evaluation. The reduced susceptibility and increased T2* at 0.55 T allowed the use of longer TRs and lower readout bandwidth. Further, an excitation flip angle of 107 deg was used to improve SNR without any additional specific absorption rate (SAR) overhead.

c. Axial T2-weighted imaging was performed using a prospectively triggered free-breathing TSE sequence for visualization of lung parenchyma. K-space was sampled using a radial trajectory to improve motion robustness compared to conventional Cartesian scanning. The slice thickness was 6 mm in 11 exams, and

5 mm in 11 exams. In order to compensate for SNR reduction with smaller slice thickness, the radial coverage factor was increased to 130%. This series was used for assessment of pulmonary groundglass and fibrosis-like opacities.

2.3. CT acquisition parameters

CT scans for each participant were acquired as a component of routine clinical care. All exams were non-contrast enhanced. Slice thickness was 1 mm in 20 exams, and 1.25 mm in two exams. All exams included the lungs in entirety, and were reviewed in lung kernel in axial plane (Visage PACS).

2.4. Imaging interpretation

Two readers, thoracic radiologists with 18 and 5 years of post-fellowship experience, were trained using two cases not included in the study. Axial T2 BLADE series, optimized for lung parenchymal visualization, were independently evaluated by each reader, blinded to patient information including other imaging. The lungs were divided into four quadrants. The right upper and middle lobes were grouped, to correspond to the similar grouping of the left upper lobe and lingula. The upper and lower lungs were scored, such that there were 4 scores per exam, for each parameter of interest.

Parameters included presence of opacity, extent of opacity, distribution of opacity, and presence versus absence of subpleural lines and subpleural reticulation. Groundglass opacity, subpleural lines, and reticulation were graded in accordance with Fleischner Society glossary of terms for thoracic imaging [16]. Extent of opacity by lung quadrant was graded on a scale of 0–4, corresponding to percentage of lobe involved: 0— no opacity; 1— <25 % opacity; 2–25-<50 % opacity; 3–50-<75 % opacity; and 4— ≥75 % opacity. Opacity distribution was graded as either peripheral (outer 1/3 lung parenchyma), central, or both. Binary grading was noted for presence or absence of parallel subpleural lines and perpendicular subpleural reticulation.

CT images at 1/1.25 mm slice thickness, displayed in a standard lung window (−600/1500) and at high-frequency reconstruction algorithm (B60) were independently evaluated by each reader, blinded to patient information including other imaging. Scoring was performed as above described. CT and MR images were reviewed at an interval of at least 3 weeks.

2.5. Statistical analyses

Agreement between readers and modalities was assessed in terms of the percentage of times concordant results were provided for the same lung quadrant. Simple kappa was used for the nominal (opacity distribution) and binary outcomes (presence of opacity, subpleural bands, and subpleural reticulation). Cohen's kappa coefficient with a linear weighted kappa was used for ordinal grading of opacity extent. The level of agreement was interpreted as poor when kappa (K) was less than zero, slight when $0 \leq K \leq 0.2$, fair when $0.2 < K \leq 0.4$, moderate when $0.4 < K \leq 0.6$, substantial when $0.6 < K \leq 0.8$, and almost perfect when $K > 0.8$. All statistical tests were conducted using SAS 9.4 (SAS Institute, Cary, NC).

3. Results

22 exams from 20 patients were included for inter-modality and CT inter-reader concordance assessments. 106 MRI exams from 64 patients (average age 53 ± 14 years, range 19–85 years; median age 55.5 years, IQR 20; 26 women) were included for MRI inter-reader concordance assessment (Table 1). Average interval between MRI and CT exams was 18 ± 9 days (range 0–30 days).

Over half of patients (39/64, 61 %) had history of prior hospital admission (mean days admitted 16 ± 17; median 8 days, IQR 16; range 1–84 days). Varying levels of oxygen support were required during acute illness among the cohort, including ECMO (n = 4), mechanical ventilation (n = 9), high flow oxygen (n = 10), simple facemask or non-rebreather (n = 1), simple nasal cannula (n = 11), and no supplemental oxygen support (n = 29). Average interval between patient-reported Covid symptom onset and MRI exam was 304 ± 138 days (median 312 days, IQR 230, range 48–569 days), or 9.5 ± 4.5 months (median 10 months, IQR 7, range 1–18 months), in this post-Covid cohort.

3.1. Inter-reader agreement for CT

On CT, inter-reader agreement was substantial for all parameters. Inter-reader concordance for detection of groundglass opacity on CT was 99 % (k = 0.96), with opacities identified in 71/88 lung quadrants by Reader 1, and 72/88 lung quadrants by Reader 2 (Table 2, Supplementary Table 2). Inter-reader concordance for extent of opacity on CT was 78 % (k = 0.86). Opacities were graded as 50 % or greater in 32/88 quadrants for Reader 1, and 27/88 quadrants for Reader 2. Greatest discordance was in extent category 2 of 25-<50 % opacity (8/88 for Reader 1, and 18/88 for Reader 2).

Characterization of opacity distribution on CT was concordant in 85/88 lung quadrants (97 %, k = 0.94), with the majority of lung quadrants demonstrating both central and peripheral opacity (Reader 1 54/88; Reader 2 55/88). Grading of presence or absence of parallel subpleural lines on CT was concordant in 87/88 lung quadrants (99 %, k = 0.97), and subpleural reticulation in 83/88 lung quadrants (94 %, k = 0.89).

3.2. Inter-reader agreement for low-field MRI

On low-field MRI, inter-reader agreement for detection of groundglass opacity was 85 % (k = 0.57), with opacities identified in 338/424 lung quadrants by Reader 1, and 320/424 lung quadrants by Reader 2 (Table 3, Supplementary Table 3). Inter-reader agreement for opacity presence was moderate to substantial in the upper lung quadrants (RUL/RML 0.58, LUL 0.63), and moderate in the lower lung quadrants (RLL 0.46, LLL 0.41).

Inter-reader concordance for extent of opacity on MRI was 48 % (k = 0.32). Opacities were graded as 50 % or greater in 70/424 zones for Reader 1, and 127/424 zones for Reader 2. While inter-reader agreement for opacity extent was fair overall (0.38), it was moderate in each lung quadrant individually (0.45–0.53, Supplementary Table 3).

Characterization of opacity distribution on MRI was concordant in 296/424 lung quadrants (70 %, k = 0.46), with the majority of lung quadrants demonstrating both central and

peripheral opacity (243/424 quadrants for Reader 1, 269/424 quadrants for Reader 2). There was moderate inter-reader concordance for characterization of opacity distribution in the upper lung quadrants (RUL/RML 0.44, LUL 0.46), and fair inter-reader concordance in the lower lung quadrants (RLL 0.29, LLL 0.25; Supplementary Table 3). Grading of presence or absence of parallel subpleural lines on MRI was concordant in 366/424 lung quadrants (86 %, k = 0.47), and grading of subpleural reticulation concordant in 321/424 lung quadrants (76 %, k = 0.37).

3.3. Concordance between CT and low-field MRI

Opacities were graded as present on CT in 19/22 exams by Reader 1 and 19/22 exams by Reader 2, and perceived on 22/22 MRI by Reader 1 and 20/22 MRI by Reader 2. Pooled inter-modality agreement for detection of groundglass opacity was moderate (86 %, k = 0.43, Table 4, Figs. 1 and 2). A higher number of lung quadrants were rated as involved by groundglass opacity on MRI (161/176) in comparison to CT (143/176).

Scoring of opacity presence was concordant between MRI and CT in 152/176 lung quadrants among readers (86 %, k = 0.43, Table 4). Inter-modality concordance for opacity extent was substantial, 0.63, with agreement in 91/176 lung quadrants (52 %). Inter-modality concordance for opacity distribution was substantial, concordant in 139/176 lung quadrants (79 %, k = 0.65). Inter-modality concordance was substantial for subpleural lines (163/176, 93 %, k = 0.8, Fig. 3), and moderate overall for subpleural reticulation (134/176, 76 %, k = 0.52, Fig. 4), though fair in the lower lung quadrants (Supplementary Table 4).

4. Discussion

We found moderate inter-modality concordance between low-field MRI and CT for detection of pulmonary groundglass opacities, with substantial concordance for grading of opacity extent, characterization of opacity distribution, and detection of subpleural bands. In the largest low-field MRI cohort to date for assessment of groundglass opacities, we found fair to moderate inter-reader agreement for opacity detection and characterization. The majority of this cohort demonstrated persisting MRI opacities an average of 9.5, and up to 18 months, after initial Covid-19 pneumonia symptom onset, highlighting the potential of low-field MRI for longitudinal surveillance.

Conventional 1.5 T MRI has demonstrated high accuracy for detection of consolidation on TSE, with sensitivity of 94 % and specificity of 98 % in a cohort of 77 outpatients with pneumonia, as compared to CT [10]. However, performance for groundglass opacities may be lower. Inter-method agreement between 3 T UTE images and CT for detection of consolidation and groundglass opacities demonstrated intraclass coefficient 0.9–1 in 23 Covid-19 patients, with higher detection rate for consolidation (100 %) than groundglass opacities (67 %) on MRI [2]. In a Covid cohort of 20 patients scanned at 1.5 T using balanced SSFP sequence, groundglass opacities were significantly less likely to be detected on MRI in comparison CT [17]. Similarly, in a Covid cohort of 52 patients imaged at 1.5 T using PD-weighted, fat-saturated TSE sequence, while inter-method concordance was high for consolidation (k = 1), it was only fair for groundglass opacities (k = 0.339) [18].

On a similar closed-bore low-field MRI system assessing groundglass opacities in a prior study, kappa concordance for opacity detection was 0.57 (present on 6 CTs and 10 MRIs) among 18 exams [9]. Our concordance between CT and MR for detection of groundglass opacity presence was k = 0.43 over 88 lung zones, in a high-prevalence cohort. Importantly, in our study, inter-modality agreement for ordinal scoring of opacity extent was substantial, 0.63. There was also substantial inter-modality agreement for additional features characterizing opacity, including distribution and subpleural bands.

Characterization of fine lung detail, the feature subpleural reticulation, showed moderate inter-modality agreement; on CT inter-reader agreement was 0.89, and 0.37 on MRI. This may in part be due the larger slice thickness used on MRI of 5–6 mm compared to the 1/1.25 mm slice thickness on CT. The near perfect inter-reader correlation on CT for all parameters, versus fair to moderate inter-reader agreement on MRI, may also be indicative of reader confidence in MR findings. Although both readers in this study were experienced in thoracic MRI, there are general limitations in knowledge regarding lung MRI in patients with prior Covid-19 pneumonia, and in relation to groundglass opacities on a low-field system.

A higher number of lung quadrants were rated as involved by groundglass opacity on T2-weighted non-contrast MR imaging sequence in comparison to CT (161 versus 143) in our cohort. Others have suggested severity of airspace abnormality may appear greater on MRI than CT [13], or alternatively, have classified the MRI findings as false positives [9] (Fig. 5). Given T2 hyperintensity may relate to edema or active inflammatory response [19–21], there is possibility that MRI is providing morphofunctional information beyond CT. This concept has been shown in other pathologies. For example, signal intensity has been correlated with disease severity in cystic fibrosis and idiopathic pulmonary fibrosis patients [20–22].

False amplification of groundglass opacities on MRI is also a possibility. Lung signal intensity may vary by sequence, for example, lung signal is higher on UTE than fast spin echo [23], and field strength [11]. Lung signal varies with patient age, and anterior-posterior location consequent gravity-dependent changes [23]. To mitigate overestimating dependent atelectasis from true groundglass opacity, we acquired T2 BLADE series early in the imaging protocol. However, even on short-duration CT exams, discerning gravity dependent change from groundglass opacity or fibrosis can be challenging without prone imaging, and has been found to be exacerbated by older age, smoking history, and obesity [24]. Similarly, we found inter-reader agreement was lower for parameters of opacity presence and distribution in the lower versus upper lung quadrants, which may relate to increased subjectivity in discerning opacities from dependent atelectasis, further affected by the peripheral predilection of Covid-19.

An additional consideration is the free breathing technique employed in this low-field MRI study. Chest CT is typically performed at full inspiration, while the MRIs in this study were performed during normal respiration with navigator-triggering, and acquisition at end-expiration. Lower lung volumes may increase lung signal due to alveolar contraction and atelectasis. Finally, increased noise related to a lower spatial and temporal resolution of MRI

may potentially increase signal. Imaging artifacts may also be more prevalent on MRI than CT.

Limitations of our study include small sample size of the inter-modality concordance analysis, restricted by shortage of temporally qualifying low-field MR and CT imaging exams. Opacities in relation prior Covid-19 pneumonia infection have been noted to persist longitudinally [14], and in absence of intervening acute illness, in similar CT distribution [15]. Our inter-modality subset of MRI and CT exams were obtained in close proximity, an average of 18 days apart, in a unique cohort with longitudinally persisting opacities. We did not adjudicate CT or MR scoring, as is often not performed in clinical scenarios, and to account for the subjectivity inherent in interpretation of even experienced radiologists. While this is the largest inter-reader evaluation of groundglass opacity detection and characterization on a low-field MRI system, further investigation will be necessary for optimization of low-field MRI sequences, including free-breathing sequences, to elucidate the value of low-field MRI for lung parenchymal evaluation.

In conclusion, low-field 0.55 T MRI demonstrates fair to moderate inter-reader concordance, and moderate to substantial inter-modality agreement with CT, for detection and characterization of groundglass and fibrosis-like lung opacities.

Supplementary Material

Refer to Web version on PubMed Central for supplementary material.

Funding

This specific research did not receive any specific grant from funding agencies in the public, commercial, or not for-profit sectors.

References

[1]. Hatabu H, Ohno Y, Gefter WB, Parraga G, Madore B, Lee KS, Altes TA, Lynch DA, Mayo JR, Seo JB, Wild JM, van Beek EJR, Schiebler ML, Kauczor H-U, Expanding Applications of Pulmonary MRI in the Clinical Evaluation of Lung Disorders: Fleischner Society Position Paper, Radiology. (2020), 201138, 10.1148/radiol.2020201138.

[2]. Yang S, Zhang Y, Shen J, Dai Y, Ling Y, Lu H, Zhang R, Ding X, Qi H, Shi Y, Zhang Z, Shan F, Clinical Potential of UTE-MRI for Assessing COVID-19: Patient- and Lesion-Based Comparative Analysis, J. Magn. Reson. Imaging 52 (2020) 397–406, 10.1002/jmri.27208. [PubMed: 32491257]

[3]. Delacoste J, Dournes G, Dunet V, Ogna A, Noirez L, Simons J, Long O, Berchier G, Stuber M, Lovis A, Beigelman-Aubry C, Ultrashort echo time imaging of the lungs under high-frequency noninvasive ventilation: A new approach to lung imaging, J. Magn. Reson. Imaging 50 (2019) 1789–1797, 10.1002/JMRI.26808. [PubMed: 31136048]

[4]. Zhu X, Chan M, Lustig M, Johnson KM, Larson PEZ, Iterative motion-compensation reconstruction ultra-short TE (iMoCo UTE) for high-resolution free-breathing pulmonary MRI, Magn. Reson. Med 83 (4) (2020) 1208–1221. [PubMed: 31565817]

[5]. Ohno Y, Koyama H, Yoshikawa T, Seki S, Takenaka D, Yui M, Lu A, Miyazaki M, Sugimura K, Pulmonary high-resolution ultrashort TE MR imaging: Comparison with thin-section standard- and low-dose computed tomography for the assessment of pulmonary parenchyma diseases, J. Magn. Reson. Imaging 43 (2016) 512–532, 10.1002/jmri.25008. [PubMed: 26223818]

[6]. Dournes G, Menut F, Macey J, Fayon M, Chateil J-F, Salel M, Corneloup O, Montaudon M, Berger P, Laurent F, Lung morphology assessment of cystic fibrosis using MRI with ultra-short echo time at submillimeter spatial resolution, Eur. Radiol 26 (11) (2016) 3811–3820. [PubMed: 26843010]

[7]. Johnson KM, Fain SB, Schiebler ML, Nagle S, Optimized 3D ultrashort echo time pulmonary MRI, Magn. Reson. Med 70 (5) (2013) 1241–1250. [PubMed: 23213020]

[8]. Hatabu H, Gaa J, Tadamura E, Edinburgh KJ, Stock KW, Garpestad E, Edelman RR, MR imaging of pulmonary parenchyma with a half-Fourier single-shot turbo spin-echo (HASTE) sequence, Eur. J. Radiol 29 (2) (1999) 152–159, 10.1016/S0720-048X(98)00167-3. [PubMed: 10374663]

[9]. Campbell-Washburn AE, Malayeri AA, Jones EC, Moss J, Fennelly KP, Olivier KN, Chen MY, T2-weighted Lung Imaging Using a 0.55-T MRI System, Radiol. Cardiothorac. Imaging 3 (2021), e200611, 10.1148/ryct.2021200611.

[10]. Syrjala H, Broas M, Ohtonen P, Jartti A, Pääkkö E, Chest magnetic resonance imaging for pneumonia diagnosis in outpatients with lower respiratory tract infection, Eur. Respir. J 49 (2017), 10.1183/13993003.01303-2016.

[11]. Campbell-Washburn AE, Ramasawmy R, Restivo MC, Bhattacharya I, Basar B, Herzka DA, Hansen MS, Rogers T, Bandettini WP, McGuirt DR, Mancini C, Grodzki D, Schneider R, Majeed W, Bhat H, Xue H, Moss J, Malayeri AA, Jones EC, Koretsky AP, Kellman P, Chen MY, Lederman RJ, Balaban RS, Opportunities in Interventional and Diagnostic Imaging by Using High-Performance Low-Field-Strength MRI, Radiology. 293 (2) (2019) 384–393, 10.1148/radiol.2019190452. [PubMed: 31573398]

[12]. Heiss R, Grodzki DM, Horger W, Uder M, Nagel AM, Bickelhaupt S, High-performance low field MRI enables visualization of persistent pulmonary damage after COVID-19, Magn. Reson. Imaging 76 (2021) 49–51, 10.1016/j.mri.2020.11.004. [PubMed: 33220447]

[13]. Campbell-Washburn AE, Suffredini AF, Chen MY, High-Performance 0.55-T Lung MRI in a Patient with COVID-19 Infection, Radiology. 299 (2021) 204155, 10.1148/radiol.2021204155.

[14]. Pan F, Yang L, Liang B, Ye T, Li L, Li L, Liu D, Wang J, Hesketh RL, Zheng C, Chest CT Patterns from Diagnosis to 1 Year of Follow-up in COVID-19, 10.1148/Radiol.2021211199. (2021). 10.1148/RADIOL.2021211199.

[15]. JJ S, B H, JP K, R C, DA L, CT of Post-Acute Lung Complications of COVID-19, Radiology. (2021) 211396. 10.1148/RADIOL.2021211396.

[16]. Hansell DM, Bankier AA, MacMahon H, McLoud TC, Müller NL, Remy J, Fleischner Society: Glossary of Terms for Thoracic Imaging, Radiology. 246 (2008) 697–722, 10.1148/radiol.2462070712. [PubMed: 18195376]

[17]. Spiro JE, Curta A, Mansournia S, Marschner CA, Maurus S, Weckbach LT, Hedderich DM, Dinkel J, Appearance of covid-19 pneumonia on 1.5 t truefisp MRI, Radiol. Bras 54 (2021), 10.1590/0100-3984.2021.0028.

[18]. Pecoraro M, Cipollari S, Marchitelli L, Messina E, Del Monte M, Galea N, Ciardi MR, Francone M, Catalano C, Panebianco V, Cross-sectional analysis of follow-up chest MRI and chest CT scans in patients previously affected by COVID-19, Radiol. Medica 126 (2021), 10.1007/s11547-021-01390-4.

[19]. Vogel-Claussen J, Renne J, Hinrichs J, Schonfeld C, Gutberlet M, Schaumann F,¨ C. Winkler, C. Faulenbach, N. Krug, F.K. Wacker, J.M. Hohlfeld, Quantification of pulmonary inflammation after segmental allergen challenge using turbo-inversion recovery-magnitude magnetic resonance imaging, Am. J. Respir. Crit. Care Med 189 (6) (2014) 650–657. [PubMed: 24401150]

[20]. Benlala I, Hocke F, Macey J, Bui S, Berger P, Laurent F, Dournes G, Quantification of MRI T2-weighted high signal volume in cystic fibrosis: A pilot study, Radiology. 294 (1) (2020) 186–196. [PubMed: 31660805]

[21]. Benlala I, Albat A, Blanchard E, Macey J, Raherison C, Benkert T, Berger P, Laurent F, Dournes G, Quantification of MRI T2 Interstitial Lung Disease Signal-Intensity Volume in Idiopathic Pulmonary Fibrosis: A Pilot Study, J. Magn. Reson. Imaging 53 (2021) 1500–1507, 10.1002/JMRI.27454. [PubMed: 33241628]

[22]. Ohno Y, Nishio M, Koyama H, Takenaka D, Takahashi M, Yoshikawa T, Matsumoto S, Obara M, Van Cauteren M, Sugimura K, Pulmonary MR imaging with ultra-short TEs: utility for disease

severity assessment of connective tissue disease patients, Eur. J. Radiol 82 (2013) 1359–1365, 10.1016/J.EJRAD.2013.02.031. [PubMed: 23523024]

[23]. Zeimpekis KG, Geiger J, Wiesinger F, Delso G, Kellenberger CJ, Three-dimensional magnetic resonance imaging ultrashort echo-time cones for assessing lung density in pediatric patients, Pediatr. Radiol 51 (1) (2021) 57–65. [PubMed: 32860525]

[24]. Kashiwabara K, Kohshi S-I, Additional computed tomography scans in the prone position to distinguish early interstitial lung disease from dependent density on helical computed tomography screening patient characteristics, Respirology. 11 (4) (2006) 482–487. [PubMed: 16771921]

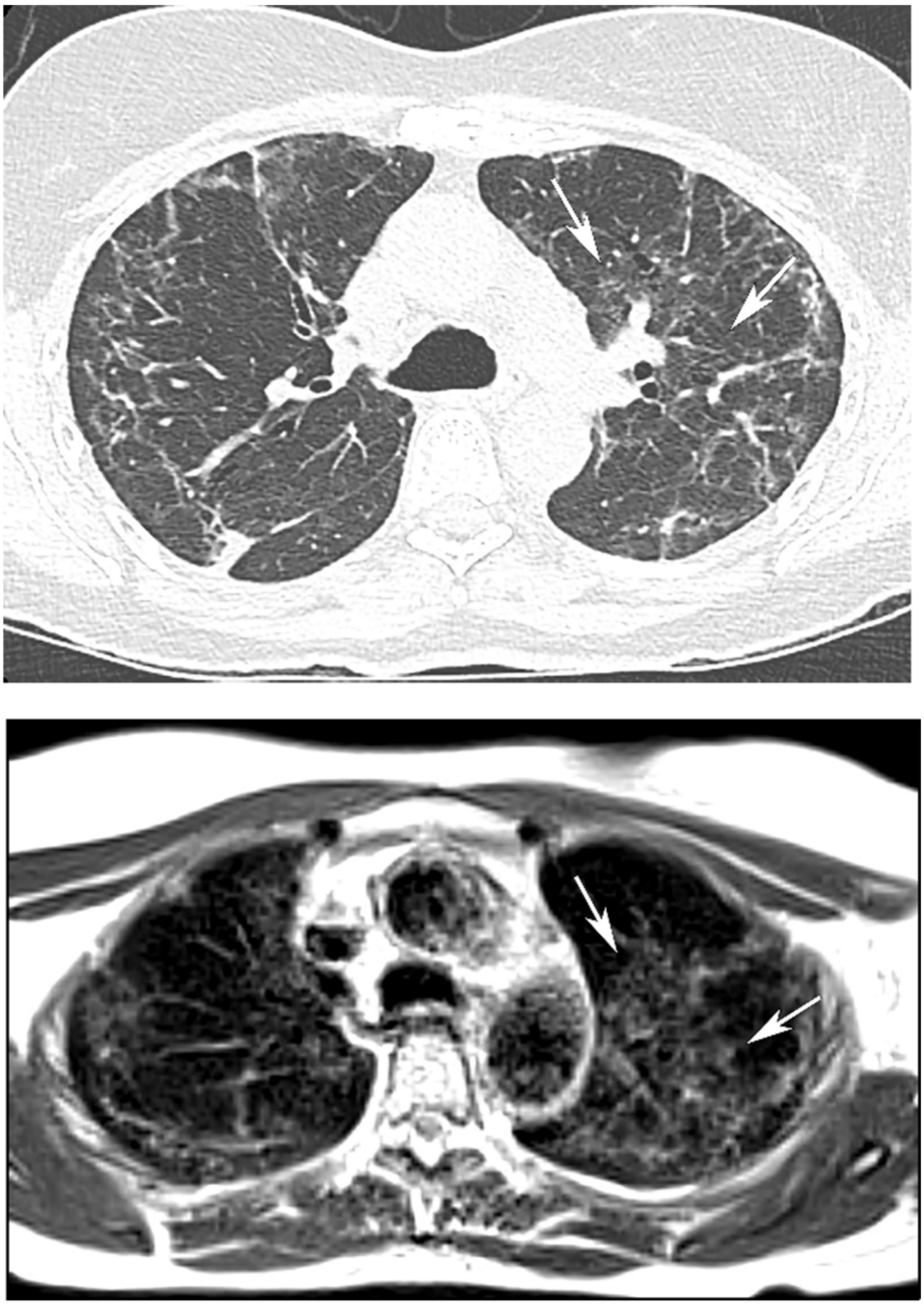

Fig. 1.

59 year old woman with history of Covid-19 pneumonia 6 months prior to MRI. (A) CT demonstrates bilateral interstitial and groundglass opacities, peripherally in the right upper lobe, and both central and peripherally in the left upper lobe. (B) MRI obtained two weeks after CT shows opacities in similar extent and distribution. Also note the sharp, geographic demarcation of the central left upper lobe groundglass medially on both CT and MRI (arrows). The AP diameter of the chest is decreased on MRI in comparison CT, which

may relate to imaging at full inspiration for CT, with quiet breathing during 5-minute MRI acquisition.

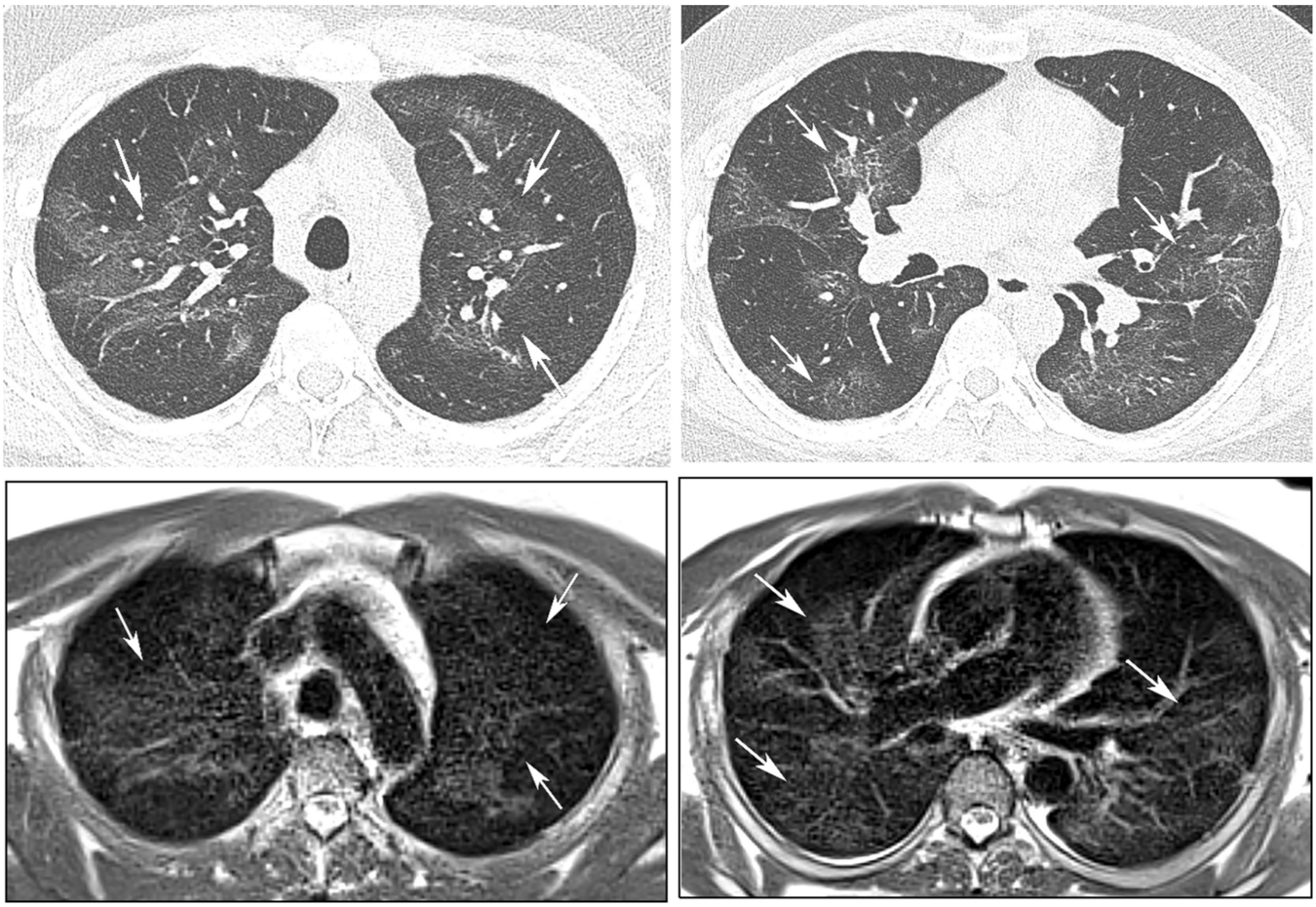

Fig. 2.

39 year old man with history of Covid-19 pneumonia 2 months prior to MRI. CT (A, B) and subsequent MRI (C, D) 6 days later demonstrate diffuse groundglass opacity the upper and mid-lungs, in similar extent and distribution (arrows).

Fig. 3.

64 year old man with history of Covid-19 pneumonia 7 months prior to MRI. A subpleural line (arrow) is conspicuous on both CT (A) and same-day MRI (B) in the basilar right lower lobe.

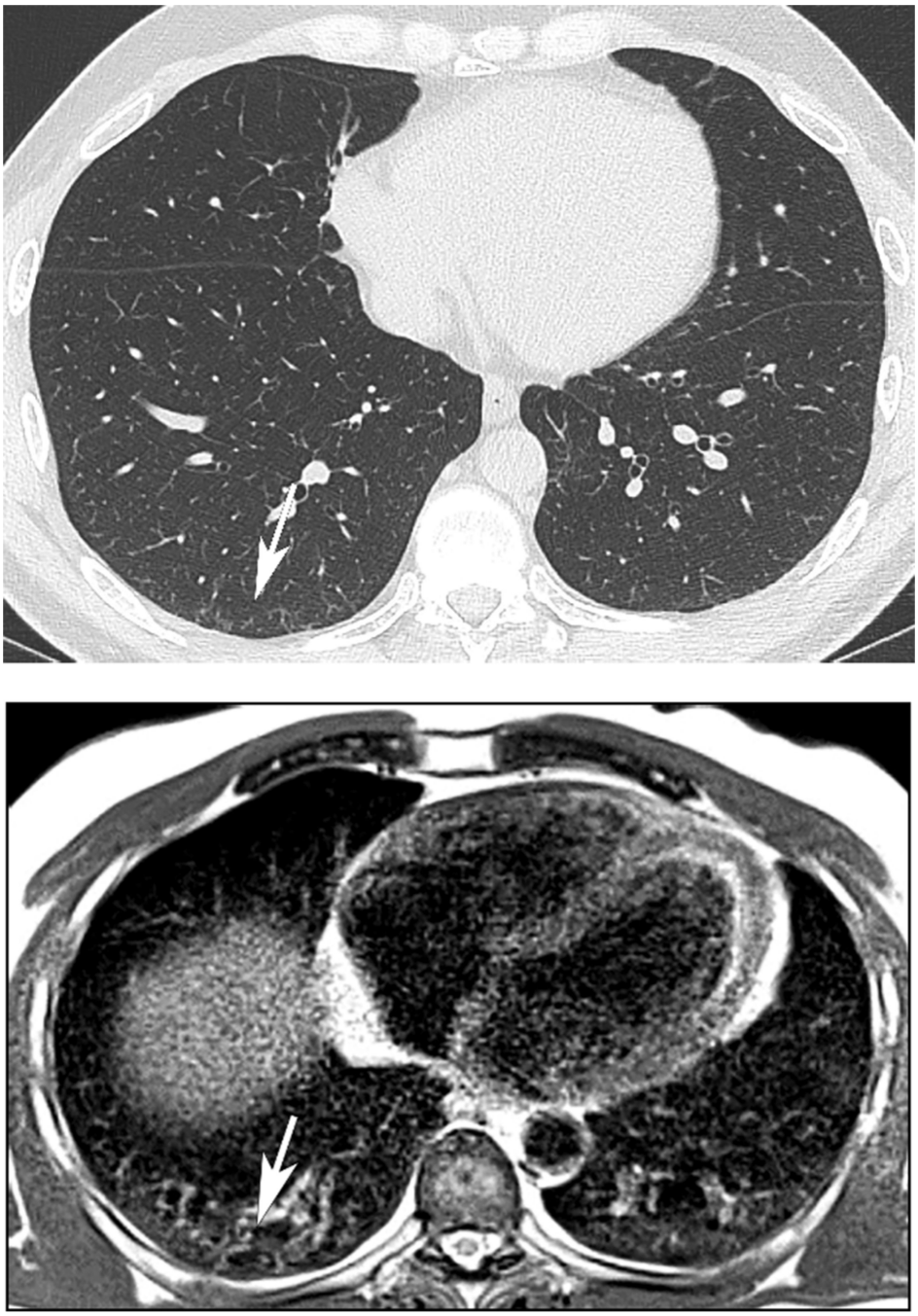

Fig. 4.

46 year old man with history of Covid-19 pneumonia 15 months prior to MRI. (A) There are subpleural reticular opacities in the right greater than left lower lobe on the companion CT (arrow), scored as present by both readers. On MRI obtained 21 days after CT, Reader 1 scored both groundglass opacities and subpleural reticulation as present in both lower lobes, while Reader 2 scored no opacities or subpleural reticular opacities to be present on MRI.

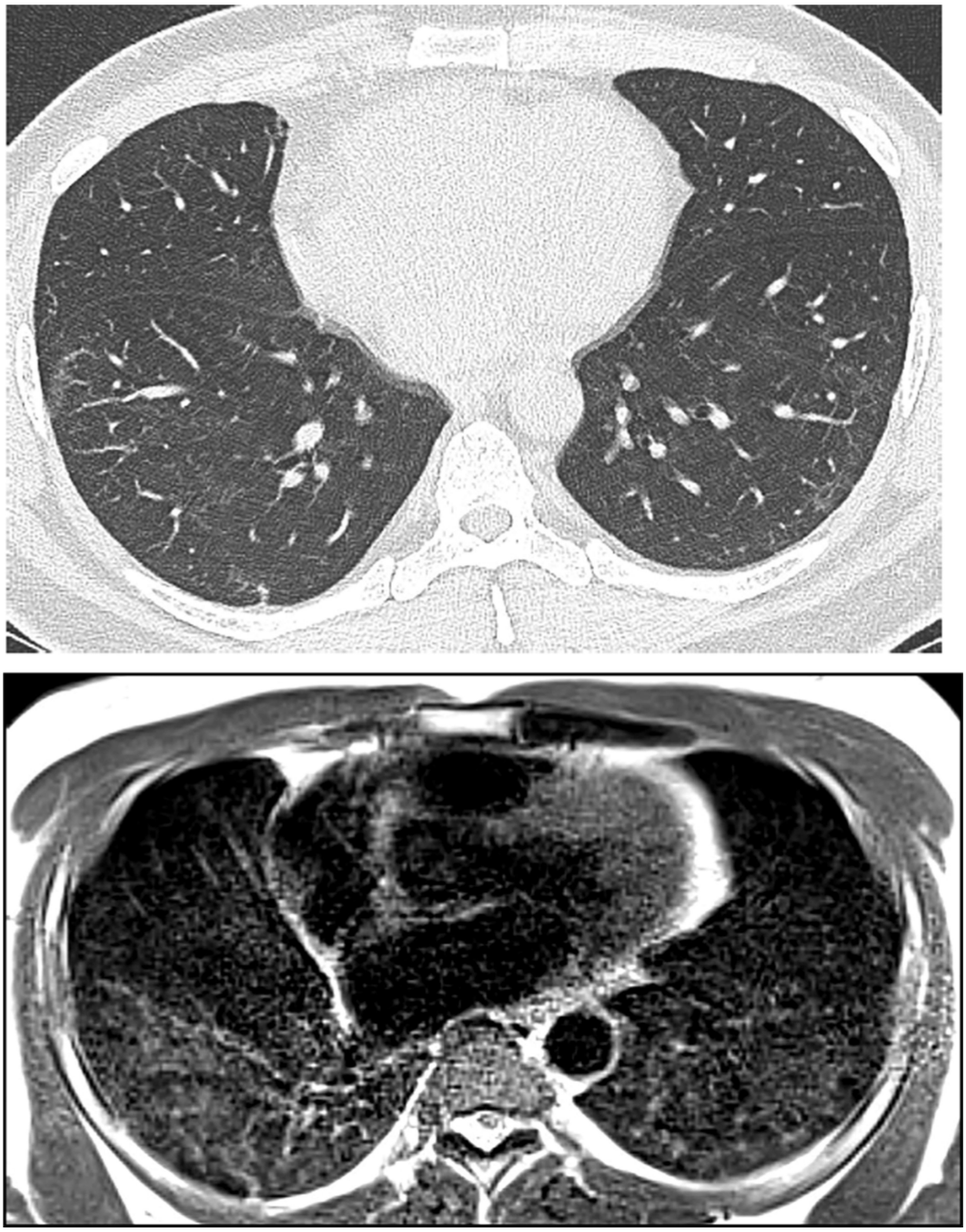

Fig. 5.

46 year old man with history of Covid 19 pneumonia 5 months prior to MRI. Right greater than left lower lobe groundglass opacity is apparent on CT (A). Low-field MRI obtained 2 days after CT demonstrates similar extent and distribution of groundglass opacity (B). Signal intensity on MRI appears to suggest greater severity of opacity than CT attenuation.

Table 1

Study Population.

	Inter-modality subset[+]	All low-field MRI exams[++]
Age in years, mean ± StDev (range)	53 ± 13 (27–76)	53 ± 14 (19–85)
Sex, n (%)		
Men	14 (70)	38 (59)
Women	6 (30)	26 (41)
Covid-19 hospital admission, n (%)	17 (85)	39 (61)
Covid-19 intubation, n (%)	7 (35)	13 (20)

[+] n =20 for sex, hospital admission, and intubation; age is calculated from age at 22 exam time points.

[++] n = 64 for sex, hospital admission, and intubation; age is calculated from age at 106 exam time points.

Table 2

Inter-Reader Concordance for CT.

Feature	Reader 1	Reader 2	Number Concordant (%) [+]	Kappa
Opacity Presence	71	72	87/88 (98.9)	0.96
Opacity Extent			69/88 (78.4)	0.86
0—no opacity	17	16		
1— <25 %	31	27		
2–25 - <50 %	8	18		
3–50 - <75 %	16	13		
4— >75 %	16	14		
Opacity Distribution			85/88 (96.6)	0.94
None	17	16		
Peripheral	16	16		
Central and	54	55		
Peripheral Central	1	1		
Subpleural Lines	23	24	87/88 (98.9)	0.97
Subpleural Reticulation	45	48	83/88 (94.3)	0.89

[+] Denominator is 88, corresponding to number of lung quadrants scored by each reader, in 22 exams.

Table 3

Inter-Reader Concordance for MRI.

Feature	Reader 1		Reader 2		Number Concordant (%) [+]		Kappa	
	Inter-modality subset[+]	All MRI[++]	Inter-modality subset[+]	All MRI[++]	Inter-modality subset[+]	All MRI[++]	Inter-modality subset	All MRI
Opacity Present	84/88 (95.5)	338/424 (79.7)	77/88 (87.5)	320/424 (75.5)	79/88 (89.8)	360/424 (84.9)	0.36	0.57
Opacity Extent					38/88 (43.2)	202/424 (47.6)	0.38	0.32
0—no opacity	4	86	11	104				
1— <25 %	32	163	26	121				
2–25 - <50 %	31	105	24	72				
3–50 - <75 %	15	51	17	86				
4— >75 %	6	19	10	41				
Opacity Distribution					73/88 (83)	296/424 (69.8)	0.55	0.46
None	4	82	9	103				
Peripheral	16	91	10	51				
Central and	67	243	69	269				
Peripheral Central	1	8	0	1				
Subpleural Lines	17	41	19	85	80/88 (90.9)	366/424 (86.3)	0.72	0.47
Subpleural Reticulation	52	125	47	94	57/88 (64.8)	321/424 (75.7)	0.29	0.37

[+]Denominator is 88, corresponding to number of lung quadrants scored by each reader, in the 22 exams used for inter-modality assessment.

[++]Denominator is 424, corresponding to number of lung quadrant scored by each reader, in all 106 low-field MRI exams.

Table 4

Inter-Modality Concordance: Comparison of Imaging Findings by 0.55 T MRI and CT.

Feature	Number Concordant (%) [+]	Kappa
Opacity Presence	152/176 (86.4)	0.43
Opacity Extent	91/176 (51.7)	0.63
Opacity Distribution	139/176 (79)	0.65
Subpleural Lines	163/176 (92.6)	0.80
Subpleural Reticulation	134/176 (76.1)	0.52

[+] Denominator is 176, corresponding to pooled scores of 88 lung quadrants per reader.